Journal of Materials Science: Materials in Electronics (2018) 29:17956–17966
https://doi.org/10.1007/s10854-018-9911-5

Systematic study of electronic properties of Fe-doped TiO_2 nanoparticles by X-ray photoemission spectroscopy

Naglaa H. S. Nasralla[1,3] · Mahboubeh Yeganeh[2] · Yayuk Astuti[1,4] · Sunthon Piticharoenphun[1,5] · Lidija Šiller[1]

Received: 2 June 2018 / Accepted: 20 August 2018 / Published online: 22 August 2018

Abstract
The importance of investigating the electronic structure of Fe doped TiO_2 nanoparticles lies in understanding their various magnetic and optical applications. In this study Fe doped TiO_2 nanoparticles were synthesized by sol–gel method in a wide range of Fe/Ti molar ratios (1, 3, 5, 8, and 10%) and post annealing at 400, 600 and 800 °C in air. The structure and size of nanoparticles were studied by X-ray diffraction and transmission electron microscopy, respectively. Systematic study of the existing states of Fe ions in Fe doped TiO_2 and transformation of the existing states as a function of annealing temperature and Fe concentration were carried out utilizing high-resolution X-ray photoemission spectroscopy (XPS). The XPS results showed that Fe was present in all samples while Fe ions were detected in mixed valence (Fe^{2+} and Fe^{3+}) states. The Fe^{3+} ions were dominant in the surface region of the nanoparticles. Moreover, the Ti in Fe:TiO_2 nanoparticles was assigned to the Ti^{4+} while a small shift towards lower binding energies was observed upon increasing the annealing temperature and dopant level. This confirms the successful incorporation of Fe into TiO_2, and the shifts in binding energies were attributed to the anatase to rutile transformation. The results verify that doping by Fe up to 10% do not exceed the limit of Fe substitutation into TiO_2 lattice.

1 Introduction

Development of nanotechnology to produce nanoparticle-based materials has provided materials with unique and tunable electronic, optical and thermal properties for different applications [1]. Among the variety of nanomaterials, nanocrystalline titanium dioxide is used in pigments, optical filters, antireflection coatings, sensors and catalysts [2]. Electronic structure and consequently magnetic and optical properties of TiO_2 nanoparticles can be changed by doping with nickel, chromium, iron, vanadium, zinc, etc. [3]. It has been revealed that photocatalytic properties and enhancement of visible light response of TiO_2 can be achieved through doping with transition metals. However, the synthesis method of nanoparticles is an important factor determining the efficiency of the photocatalytic process. There are different methods for synthesis of Fe doped TiO_2 including sol–gel [4], hydrothermal [5], combining sol–gel method with hydrothermal treatment [6] and etc. Due to similarity between ionic radii of Fe^{3+} and Ti^{4+} (0.064 and 0.068 nm, respectively), iron is one of the best doping materials in which Fe^{3+} ions can be possibly located at interstice positions or within the lattice [7].

Since detection of room temperature ferromagnetism (FM) in Co:TiO_2 [8], numerous studies have been performed to investigate the magnetic properties of TiO_2 nanoparticles doped with transition metals [4, and references therein]. Magnetic properties of Fe doped TiO_2 at Fe/Ti molar ratio of 1 and 5% were investigated by SQUID magnetometry in our previous study [4] and ferromagnetic order with T_c about 350 K was observed in TiO_2 sample doped by 5%

✉ Mahboubeh Yeganeh
Mahboubeh.yeganeh@yahoo.co.uk

✉ Lidija Šiller
Lidija.Siller@ncl.ac.uk

1 School of Chemical Engineering and Advanced Materials, Newcastle University, Newcastle upon Tyne NE1 7RU, UK

2 School of Natural Science, Kosar University of Bojnord, P. O. Box 94104455, Bojnord, Iran

3 Physics Division, Electron Microscope and Thin Film Department, National Research Centre, Dokki, Giza 12622, Egypt

4 Chemistry Department, Faculty of Science and Mathematics, Diponegoro University, Semarang, Central Java 50275, Indonesia

5 Department of Chemical Engineering, Silpakorn University, Bangkok, Thailand

Fe and annealed at 800 °C. Despite numerous studies were performed in different physical properties of Fe doped TiO_2, controversial results have been reported [9–11]. Inconsistency of the results can be due to the multiple factors such as synthesis method, annealing temperature and iron content.

It has been revealed that physical properties of Fe dope TiO_2 strongly depend on the structural modifications associated to iron incorporation as a dopant (interstitial or substitutional) and possible hematite segregation. The segregation can be a disadvantage and result the poor photocatalytic activity; therefore controlling the dopant seems to be essential [7]. The segregation can be happened when iron concentration exceeds the limit of substitution into TiO_2 lattice, and again controversial results were found in literature. Ganesh et al. [12] found the existence of α-Fe_2O_3 and $FeTiO_3$ when Fe content was ≥ 4 wt%. Zhu et al. [13] recognized α-Fe_2O_3 for iron ≥ 5 wt%, while Crisan et al. [9] reported completely solubilized Fe (up to 5 wt%) in anatase lattice.

Although there is much doubt about the origin of observed ferromagnetism in transition metal doped TiO_2, some researchers claimed that FM can be originated from clustering or impurities while some others strongly supported the intrinsic origin of FM behaviour which has been initiated by the presence of defects such as oxygen vacancies [14]. It has been suggested that doping by Fe^{3+} can create more oxygen vacancies into crystal lattice and on the surface of TiO_2 leading to the enhancement of photocatalytic activities and magnetic properties [9, 11, 15]. On the other hand, XRD was typically used in most studies to determine Fe substitution into TiO_2 lattice [16, 17]. As this technique can not yield definitive evidence for dopant substitution due to its detect limitation and the possibility of existing amorphous phase of Fe [18], investigating of the changes on the photoelectron peak shape of TiO_2 due to addition of dopant is of particular interest.

In spite of importance of mentioned subject, there are few studies that have systematically investigated the existing states of Fe ions and transformation of these states at different annealing temperatures and Fe concentrations in Fe doped TiO_2. Therefore by considering the importance of iron incorporation into TiO_2 lattice as a dopant, further detailed investigations on electronic properties of Fe:TiO_2 and their changes due to annealing temperature and doping concentration are critical.

In this work, we mainly focus on studying the effects of chemical environments (structure, annealing temperature, dopant level) on core electron levels and the bond type that they formed as well as understanding the composition and electronic state of the surface using high resolution X-ray photoelectron spectroscopy (XPS). The XPS of Fe doped TiO_2 has been investigated by some groups [9, 19–21]. However, since the 2p core electron level spectra exhibits asymmetry due to the multiplet splitting and shake-up processes [22, 23], the analysis of the XPS spectra of of transition metals and their oxides is very complex. In addition, the fittings of the XPS curves of Fe-doped TiO_2 nanoparticles found in the literature, have not been enough accurate often neglecting the multiplet splitting, surface and satellite structures contributions or ignoring the necessary use of the doublet functions to fit 2p spectra, causing the inconsistency of the described results by different groups [19, 24–26].

In order to systematically study the effects of chemical environments on the core electrons binding energies which depend on the crystalline structure, size of the particles and their morphology, high resolution XPS were performed in a wide range of Fe doping level (1, 3, 5, 8 and 10%) at different annealing temperatures (400, 600 and 800 °C). Sol–gel synthesis method has been utilized for preparation of the samples as the concentration of dopant can be controlled by this technique. Then, the high-resolution XPS spectra of Ti 2p, O 1s, and Fe 2p electronic core levels were recorded for more detailed analysis. The XPS curve fittings of 2p core levels were performed by considering multiplet splittings, surface and satellite structure contributions using necessary doublet functions.

2 Experimental procedure

Fe doped TiO_2 nanoparticles at different Ti/Fe molar ratios (1, 3, 5, 8 and 10%) were prepared by sol–gel method as described in our earlier work [4]. The post annealing of the samples were performed at 400, 600 and 800 °C in air. The X-ray diffraction (XRD) spectroscopy was applied to study the structure of Fe doped TiO_2 nanoparticles. The XRD analysis was carried out via utilizing a D8 Advance Bruker system, using Cu Kα1 (λ = 0.154056 nm) radiation while 2θ was varying from 20 to 70. Transmission electron microscopy (TEM) micrographs of the prepared nanopowder were recorded using a JEOL 2100F field emission gun transmission electron microscope (FEG TEM) operating at 200 keV. High resolution XPS spectra were measured by a Scienta ESCA 300 photoelectron spectrometer at the National Centre for Electron Spectroscopy and Surface Analysis (NCESS), Daresbury Laboratory, UK. This incorporates a rotating anode Al $K\alpha$ ($h\upsilon = 1486.6$ eV) X-ray source, a seven crystal X-ray monochromator and a 300 mm mean radius spherical sector electron energy analyser with parallel electron detection system. The X-ray source operated at 200 mA emission current and 14 kV anode bias, while the analyser run at 150 eV pass energy for survey spectra and at 20 eV pass energy for core level spectra, with 0.8 mm slits. All measurements were obtained at a pressure ~ 10^{-9} Torr. Samples were mounted by a double-sided carbon tape in a transferable sample holder while charging was compensated with an electron flood gun.

The binding energy of the spectra was referenced to the residual C 1s of amorphous carbon which has been assigned to a binding energy of 284.6 [27]. Collected XPS spectra were fitted by Winspec software. All Fe 2p core levels were fitted using a Doniac-Šunjic line shape [28] convoluted with a Gaussian profile, while the fitting of the other core level peaks were achieved by the Lorentzian form convoluted with the same Gaussian. The Gaussian component considers the instrumental energy resolution and also chemical disorder, while the Lorentzian explains the lifetime of the photoionization process [29]. Shirley method was used to subtract the photoelectron background [30].

3 Results and discussion

The XRD patterns of 1 and 5% of Fe doped TiO_2 were presented in our previous work [4] and the XRD pattern corresponding to 10% Fe (molar ratio) was shown in Fig. 1. XRD results were compared to the standard JCPDS card no: 89-4920 and JCPDS card no: 89-4921 databases for rutile and anatase TiO_2, respectively. The results revealed the existence of both anatase and rutile phase with the dominance of anatase at annealing temperature of 400 °C. Further increase in annealing temperature to 600 °C leads to the dominance of rutile phase over anatase. Finally, the anatase phase was disappeared at annealing temperature of 800 °C and the monostructure rutile phase for all concentrations of Fe was observed except for 10% Fe doped TiO_2 nanoaprticles annealed at 800 °C, whereas pseudobrookite phase co-exist with the rutile phase. XRD patterns did not show any diffraction peaks of iron suggesting the need for further study to verify the formation of an iron–titanium solid solution and the incorporation of Fe into the TiO2 crystal structure substitutionally. As confirmed by XRD patterns (Fig. 2) and the summarized results in Table 1, the major effect of doping by iron was a decrease in the anatase phase and consequently an increase in the rutile upon increasing the iron concentration.

TEM images of 5% Fe doped TiO_2 annealed at 400 and 800 °C are illustrated in Fig. 3. Table 1 shows the measured size by TEM of the all synthesized samples in this work. A significant increase in growth of crystallite size was observed following the phase transformation from anatase to rutile. However, at higher Fe concentrations, a decrease in the particle size was observed which can be possibly attributed to the reduction of the kinetics of particle growth at higher annealing temperature by increasing the Fe concentration. This could be explained by the presence of Fe^{3+} at the surface of TiO_2 nanoparticles (as it will be shown), leading to a decrease in surface energy and thermodynamic driving force for particle growth [15].

XPS study which forms the main part of this work was performed to obtain the spectra of Ti 2p, O 1s and Fe 2p core levels. The Ti 2p photoemission spectrums of 8 and 10% (molar ratio) Fe doped TiO_2 nanoparticles annealed at 400, 600 and 800 °C were presented in Fig. 4a, b, respectively. Table 2 summarizes the observed changes in the binding energy of Ti 2p photoemission spectrum when Fe concentration increases from 1 to 10% and annealing temperature varied from 400 to 800 °C. The binding energies shifted from 458.7 to 458.0 eV and peak separations changed from 5.86 to 5.65 eV. The XPS data of Fe:TiO_2 nanoparticles indicated that the Ti 2p spectrum are symmetric without the shoulder [31] and Ti was assigned to the Ti^{4+} (TiO_2) [32].

A mean value of 458.7 eV was attributed to the position of the Ti^{4+} of Ti 2p spectrum by Mayer et al. [33] after

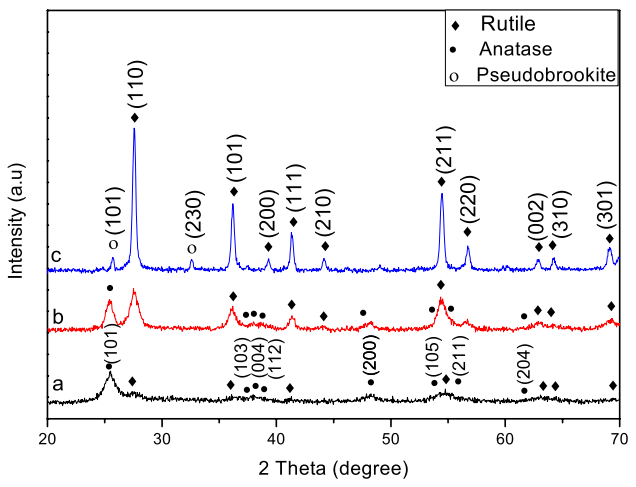

Fig. 1 XRD patterns of 10% Fe:TiO_2 nanoparticles as a function of annealing temperatures at: a 400 °C, b 600 °C, and c 800 °C

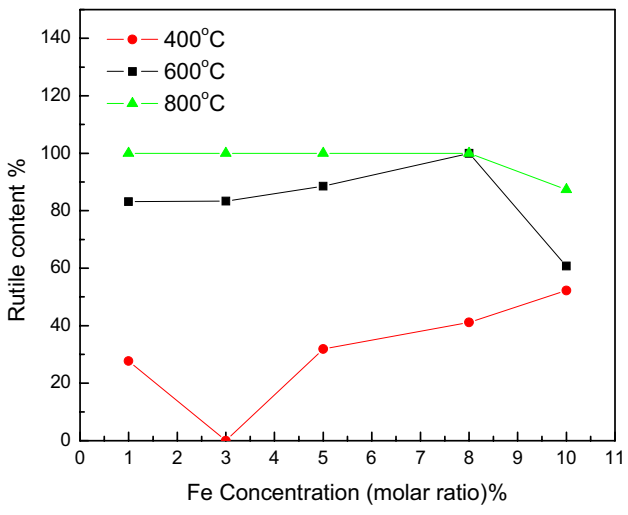

Fig. 2 Rutile content (±5%) as a function of various annealing temperatures and Fe concentrations

Table 1 Measured particle size by TEM for Fe:TiO_2 at different temperatures and iron concentrations, phase identification and rutile content (%)

Dopant ratio (Fe/Ti)%	Annealing temperature (°C)	Particle size (nm)	Phase identification	Rutile content (%) (±5%)
1	400	10–14	Anatase Rutile	27.73
1	600	13–20	Anatase Rutile	83.16
1	800	50–97	Rutile	100
3	400	18–40	Anatase Rutile	0
3	600	14–34	Anatase Rutile	83.38
3	800	49–88	Rutile	100
5	400	6–10	Anatase	31.9
5	600	22–30	Anatase Rutile	88.55
5	800	50–100	Anatase Rutile	100
8	400	30–49	Anatase Rutile	41.16
8	600	13–34	Rutile	100
8	800	33–76	Rutile	100
10	400	33–100	Anatase Rutile	52.2
10	600	7–33	Anatase Rutile	60.74
10	800	21–27	Pseudobrookite Rutile	87.36

considering the results of 16 different research groups. The binding energy of Ti^{4+} in Ti 2p spectra of single-crystal of rutile (110) surface was found at 459.3 eV [34]. However, it has been observed that upon surface annealing, the TiO_2 surface reduction and point defects are generated in the rows of bridging oxygen atoms [34]. Due to the presence of oxygen vacancies, the extra electrons in vacancies cooperate as the donor-like states that accumulate as a layer in near-surface region causing the downwards band-bending. It was found that after adsorption of oxygen gas at room temperature, these defects disappear, but an upward shift of all peaks by ~ 0.2–0.3 eV is resulted [34]. Figure 4 and Table 2 show that the Ti 2p peak positions shifted towards lower binding energy with increasing the Fe content and annealing temperature from 400 to 800 °C. As mentioned above, annealing at high temperature creates oxygen vacancies leading to core electron levels shift towards lower binding energies [15, 34]. It is also worth mentioning that the increasing level of oxygen vacancies, can also assist the structural rearrangement from the anatase to the rutile [35].

The phase content of the samples were estimated by Spurr and Myers method [36] in accordance with the following equation:

$$X_A = 1 - X_R = \left(1 + 1.26 \times I_{27.5}/I_{25.3}\right)^{-1}$$

where the subscripts (A) and (R) indicate the anatase and rutile phase, respectively. $I_{27.5}$ and $I_{25.3}$ are the relative intensity of the rutile (110) peak at 2θ ~ 27.5° and the anatase (101) at 2θ ~ 25.3°. As Fig. 2 shows, the rutile phase quantity almost increased by raising the annealing temperatures from 400 to 800 °C which is in agreement with literature [37, 38]. The same trend was observed by increasing the Fe concentration from 1 to 8%, apart from 10% Fe annealed at 800 °C due to the appearance of the pseudobrookite phase.

The anatase has more distorted structure than rutile. Two of the titanium–oxygen bonds are longer than the others and the O–Ti–O bond angles in anatase deviate more from 90 in comparison to rutile [34]. Ti atoms in rutile TiO_2 are in an octahedral (Oh) coordination environment [34]. Therefore, the shifts in the binding energies of core electron levels can

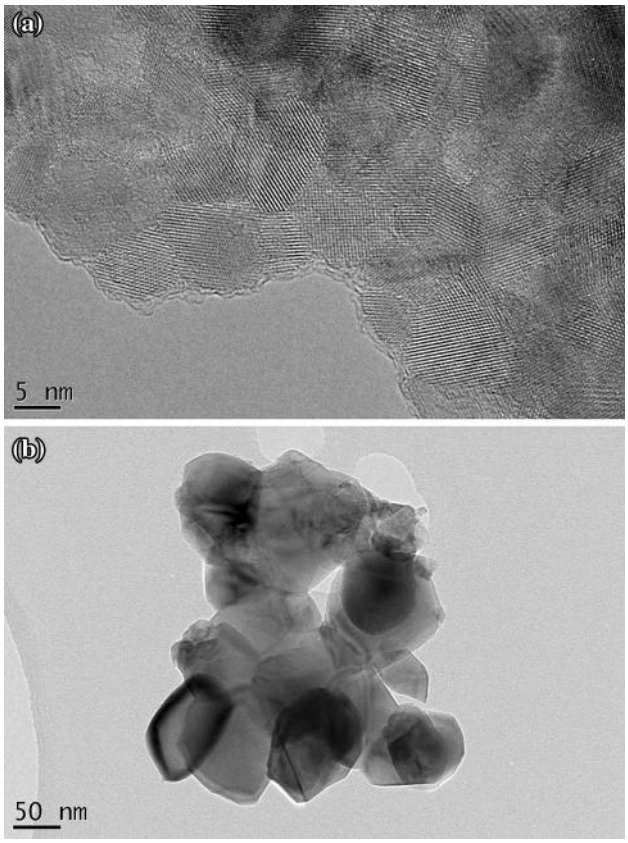

Fig. 3 TEM image of 5% Fe concentration at: **a** 400 °C and **b** 800 °C

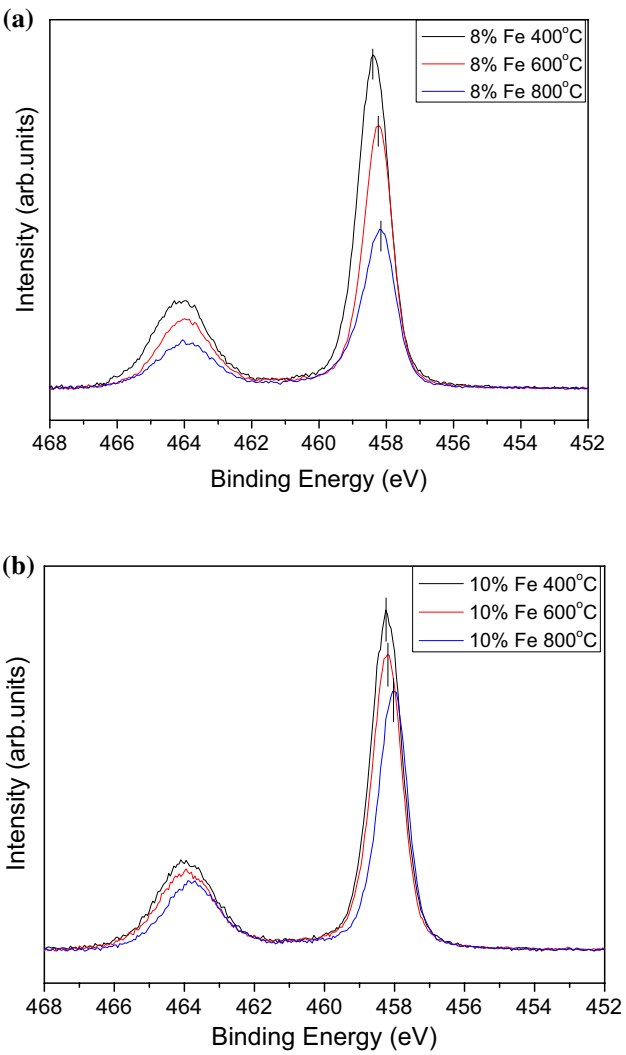

Fig. 4 XPS core level Ti 2p spectrum of **a** 3% and **b** 10% Fe doped TiO_2 annealed at 400 °C, 600 °C, and 800 °C in air

also be attributed to transformation of crystal structures from the anatase to rutile phase.

The obtained binding energies of the O 1s region of all prepared samples were described in Table 3. The spectra of samples containing 1, 3 and 10% Fe were represented in Fig. 5.

It is notable that O 1s spectrums of all samples were asymmetric which indicate the presence of more components, such as hydroxyl groups, on TiO_2 surface [9]. The O 1s spectra was fitted with two or three peaks in which the lowest binding energy peak ranges from 529.40 to 529.90 eV was attributed to the lattice oxygen in TiO_2 [20, 39, 40]. The second peak with higher binding energy ranging from 530.1 to 530.9 eV was assigned to the chemisorbed oxygen related species such as hydroxyl groups and to the located oxygen vacancies at the particles surface. The third peak range from 531.6 to 532.1 eV was also attributed to the adsorbed water [20, 40–42]. It has been reported that hydroxyl groups (i.e. Ti–OH and H_2O) are strongly bound to surface defects on anatase and rutile surfaces annealing at different temperatures [10]. Increasing annealing temperature from 400 to 800 °C can reduce the number of surface hydroxyl groups per surface area of TiO_2 [10, 43] while increasing dopant level can enhance the oxygen vacancies. It can be noticed

Table 2 Binding energy (eV) for Ti $2p_{3/2}$ (with its spin–orbit splitting value) in 1%, 3%, 5%, 8% and 10% Fe doped TiO_2 annealed at 400 °C, 600 °C, and 800 °C in air. Data corresponding to 1 and 5% Fe was originated from [4]

Iron concentration	Binding energy (peak separation) (eV)		
	At 400 °C	At 600 °C	At 800 °C
1% Fe	458.7 (5.7)	458.5 (5.7)	458.1 (5.7)
3% Fe	458.6 (5.8)	458.4 (5.7)	458.2 (5.7)
5% Fe	458.4 (5.7)	458.4 (5.8)	458.3 (5.8)
8% Fe	458.4 (5.7)	458.2 (5.8)	458.1 (5.8)
10% Fe	458.2 (5.7)	458.2 (5.8)	458.0 (5.9)

that the content ratio of the second peak (described above) of the samples annealed at 400 °C increased when the Fe concentration changed from 1 to 3%. This can be explained

Table 3 The binding energies (B.E.) of O 1s components of different Fe doped samples in (eV)

Sample	O^{2-}		OH^-		H_2O	
	B.E. (FWHM)	Ratio%	B.E. (FWHM)	Ratio%	B.E. (FWHM)	Ratio%
1% Fe_400 °C	529.9 (1.28)	72.44	530.5 (2.59)	27.56	–	–
1% Fe_600 °C	529.7 (1.47)	84.51	530.9 (2.5)	15.49	–	–
1% Fe_800 °C	529.4 (1.43)	83.06	530.7 (1.64)	13.75	532.1 (1.29)	3.18
3% Fe_400 °C	529.8 (1.22)	61.67	530.6 (2.37)	38.33	–	–
3% Fe_600 °C	529.6 (0.98)	71.00	530.3 (1.34)	24.25	531.6 (1.21)	4.76
3% Fe_800 °C	529.4 (1.01)	44.53	529.9 (1.84)	39.68	531.8 (1.38)	15.78
5% Fe_400 °C	529.7 (1.42)	71.29	530.3 (3.01)	28.71	–	–
5% Fe_600 °C	529.5 (1.26)	81.77	530.6 (1.76)	10.79	531.7 (2.03)	7.45
5% Fe_800 °C	529.6 (1.97)	67.4	530.6 (1.89)	26.04	531.8 (1.97)	6.56
8% Fe_400 °C	529.6 (1.14)	73.12	530.7 (2.56)	26.88	–	–
8% Fe_600 °C	529.48 (1.01)	48.85	529.98 (1.61)	36.05	531.74 (1.43)	15.10
8% Fe_800 °C	529.40 (1.1)	47.82	530.12 (1.58)	31.74	531.71 (1.48)	20.44
10% Fe_400 °C	529.57 (1.14)	78.17	531.16 (2.31)	21.83	–	–
10% Fe_600 °C	529.5 (1.016)	52.89	530.1 (1.44)	32.95	531.7 (1.47)	14.15
10% Fe_800 °C	529.4 (1.08)	70.96	530.3 (1.82)	16.65	531.9 (1.35)	12.38

by increasing oxygen vacancies. At higher Fe concentration, iron starts to diffuse to interior leading to the decrease in the content ratio of this peak and this reduction is getting more pronounced at 10% Fe level. The same results were achieved for the samples annealed at 600 and 800 °C.

Figure 6 presents the high resolution XPS spectra of Fe 2p region of the prepared Fe-doped TiO_2 nanoparticles. Curve fittings for the various chemical states of 1, 3 and 10% (molar ratio) Fe doped TiO_2 nanoparticles were presented in Figs. 7, 8 and 9, respectively. As can be observed, all samples are richer in Fe^{3+} oxidation state than Fe^{2+} state. By taking into consideration that initial sol–gel was prepared with Iron(III) chloride 6-hydrate, it was expected that Fe would contain mainly +3 oxidative state (Fe^{3+}) [44]. It has been reported that binding energies for Fe^{3+} and Fe^{2+} states are at 710.9 eV and 709.4 eV, respectively [32]. Table 4 contains all binding energies, full width at half-maximum values and oxidation states of Fe in TiO_2 nanoparticles.

The existence of two chemical states of iron (Fe^{3+} and Fe^{2+}) with small portion of Fe^{2+} can be explained by the presence of residual carbon from organic radicals, introduced by molecular precursors. Following thermal treatment, this residual carbon could draw oxygen from the surrounding atmosphere during oxidation process causing the reduction of Fe^{3+} oxidation state to Fe^{2+} oxidation state [45]. However Yen et al. [46] explained the coexisting of the Fe^{2+} and Fe^{3+} as a consequence of the reduction by generated electrons due to incident of light on the Fe doped TiO_2. Almost all Fe-doped TiO_2 samples annealed at 400, 600 and 800 °C consisted of Fe^{2+} and Fe^{3+} except sample with 1% Fe at 400 °C in which the Fe 2p spectra of this sample shows two additional peaks at 705.9 eV and 708.47 eV. This might be due to two possibilities. Firstly, peaks at 705.9 and 708.47 eV may be assigned to Fe^0 and Fe_3O_4, respectively [47], on the basis of the thermodynamics of Fe. Specifically, it is known that below 575 °C, iron oxide (FeO) is thermodynamically unstable and dissociates into metallic Fe and Fe_3O_4, the later will give Fe^{3+} by annealing [48]. Secondly the lower intensity peak at 705.9 eV can be due to defects which are formed during sample preparation [49].

It can be deduced from Table 4 that Fe^{3+} peak positions shift towards higher binding energies upon increasing annealing temperature from 400 to 800 °C. The observed positive shift in the binding energy and an increase in intensity of Fe^{3+} component can be attributed to high annealing temperatures and prolonged times (at 400, 600, and 800 °C for 1 h in air). The high annealing temperature results in oxidation of Fe^{2+} into Fe^{3+} [47], diffusion of Fe ions in substitutional positions of the TiO_2 crystal lattice and formation of Ti–O–Fe complexes in Fe–TiO_2 [50]. In all spectra, the Fe $2p_{3/2}$ peak exhibits an asymmetric tail at higher binding energies which can be assigned to the surface contribution of nanoparticles in XPS having different binding energies compared to that of the bulk nanostructure [51]. The discrepancy between the surface and bulk binding energies was attributed to a decrease in the crystal field energy of Fe ions located at the surface (top two layer) and in contrast to those located within the bulk [52], it can be detected when high resolution XPS is used [53].

In summary XPS results confirmed the presence of Fe in all prepared Fe doped TiO_2 nanoparticles, despite observing no signal of Fe in the XRD patterns. Doping with Fe has two effects on TiO_2 lattice. It can facilitate the anatase to rutile transformation rate and also, as stated by Wu et al. [15], Fe^{3+} can establish the charge compensation by creating more oxygen vacancies which could be responsible for the

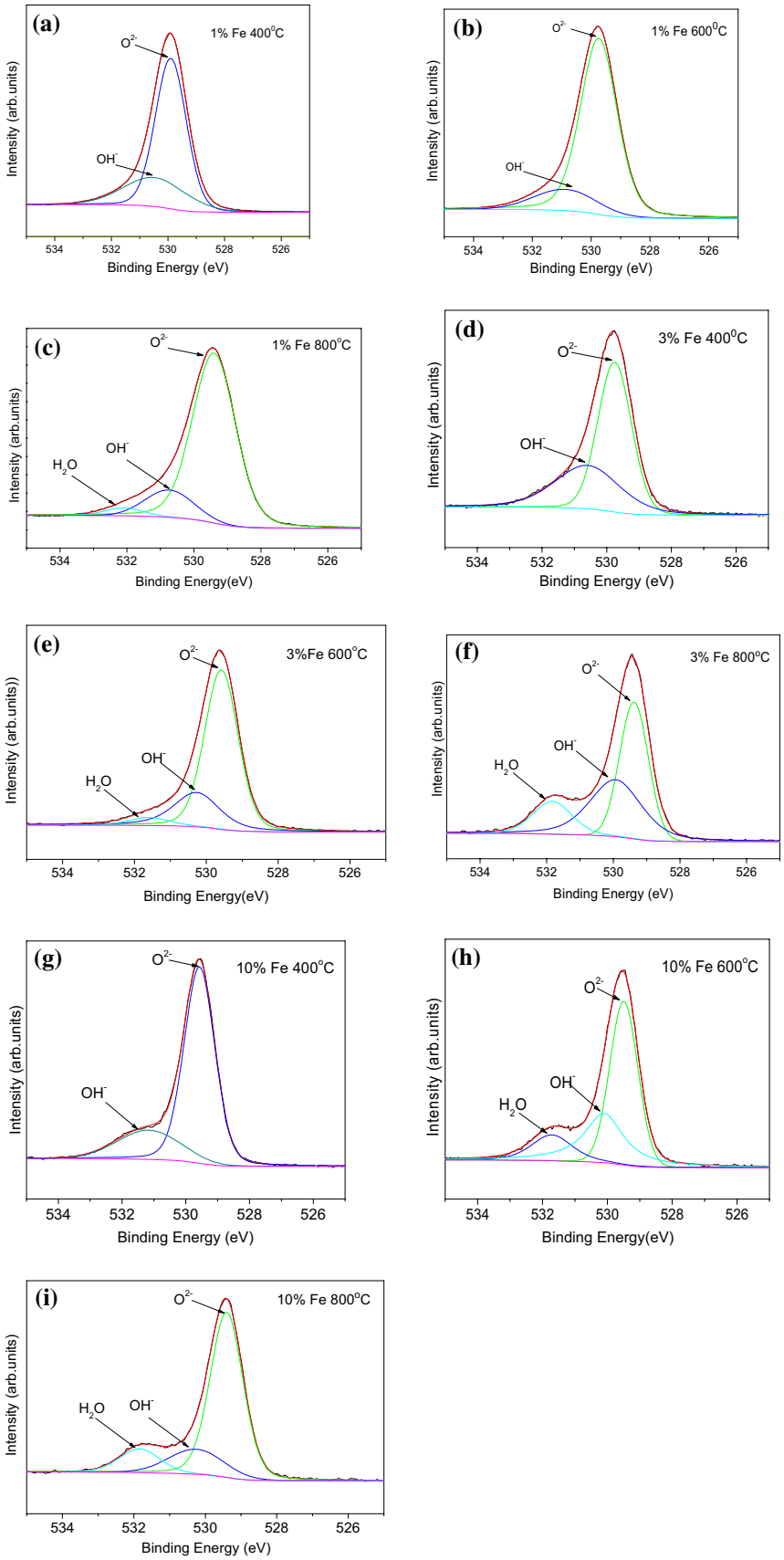

Fig. 5 XPS core level spectra of the O 1s region of 1%, 3% and 10% Fe-doped TiO_2 annealed at 400 °C, 600 °C and 800 °C in air

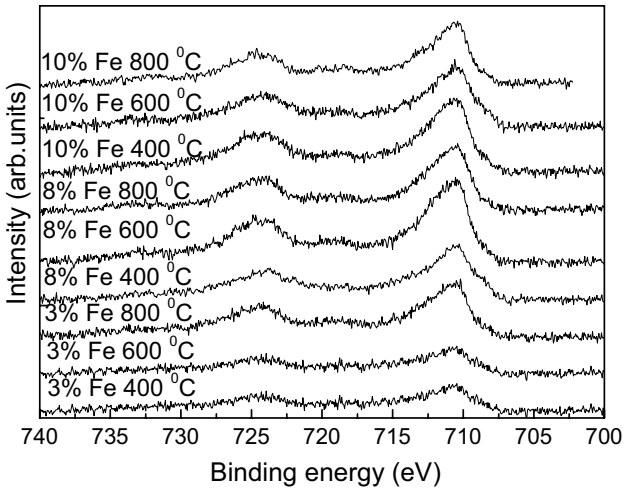

Fig. 6 XPS core level spectra of the Fe 2p region of 3, 8 and 10% Fe-doped TiO_2 annealed at 400 °C, 600 °C, and 800 °C

observed magnetic behaviour in Fe doped TiO_2 [4, 11, 54]. The substitution of Fe into TiO_2 lattice was confirmed by negative shift in the binding energies of Ti $2p_{3/2}$ core levels.

In this work, a series of Fe doped TiO_2 at different Fe concentration and annealing temperature were synthesized and studied by XPS in order to achieve a complementary data regarding the structural and electronic properties of the samples. Utilizing the high resolution XPS has provided additional information on discrepancy between the surface and bulk binding energies. In addition, systematic study on the existing states of Fe ions in Fe doped TiO_2 and transformation of the existing states by increasing the annealing temperature and Fe concentration was performed.

Despite the literature reports regarding the observation of Fe segregation [12, 13], Fe ions in this work, were doped into TiO_2 lattice and Fe concentration up to 10% did not exceed the saturation limit.

4 Conclusion

The physical properties of Fe doped TiO_2 can be changed when iron incorporates in interstitial or substitutional mode or when possible hematite segregation occurs. The segregation can be occurred when iron exceeds the limit of substitution into TiO_2 lattice. Indeed, the incorporation of Fe in substitutional mode is highly desired in most applications. In this work, Fe doping to TiO_2 nanoparticles were detected using XPS, while they were not identified by XRD and TEM. The successful incorporation of Fe into the TiO_2 lattice of different samples of Fe:TiO_2, prepared in wide range of Fe concentration (1, 3, 5, 8 and 10%) and annealing temperature (400, 600 and 800 °C), was confirmed by small negative shift of binding energy of Ti 2p when the annealing

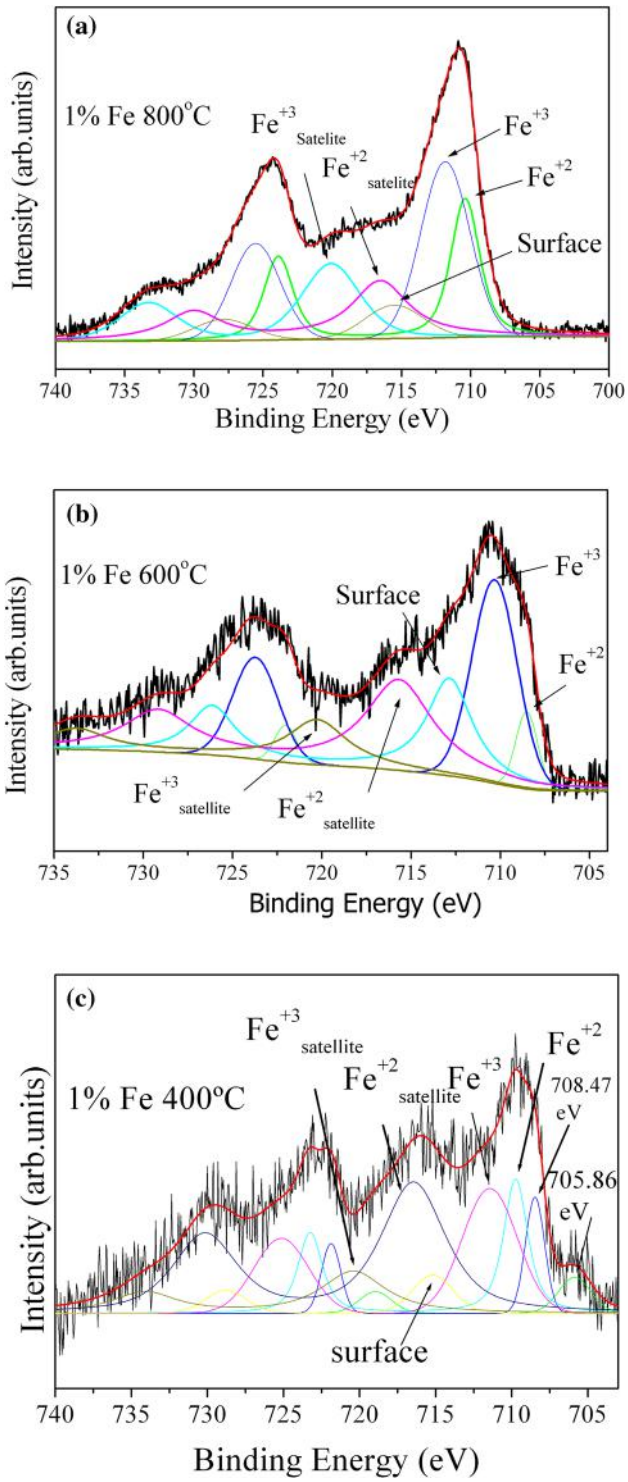

Fig. 7 High resolution XPS core level spectrum of 1% Fe annealed at 800 °C, 600 °C, and 400 °C. Data corresponding to 1% Fe annealed at 800 °C was reproduced from [4]

temperature and the Fe concentration were increasing [33, 34]. Furthermore, oxidation states of Fe ions were determined in mixed valence (Fe^{2+} and Fe^{3+}) states. The Fe^{3+}

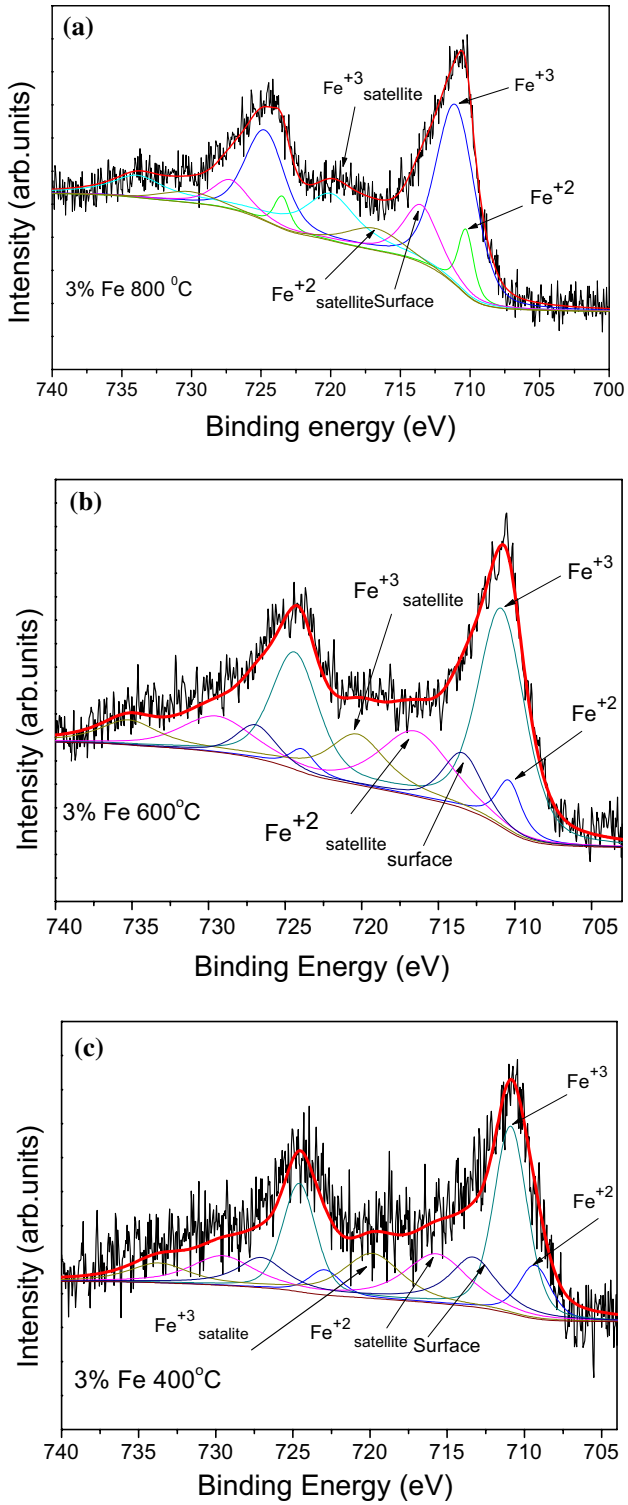

Fig. 8 High resolution XPS core level spectrum of 3% Fe annealed at 800 °C, 600 °C, and 400 °C

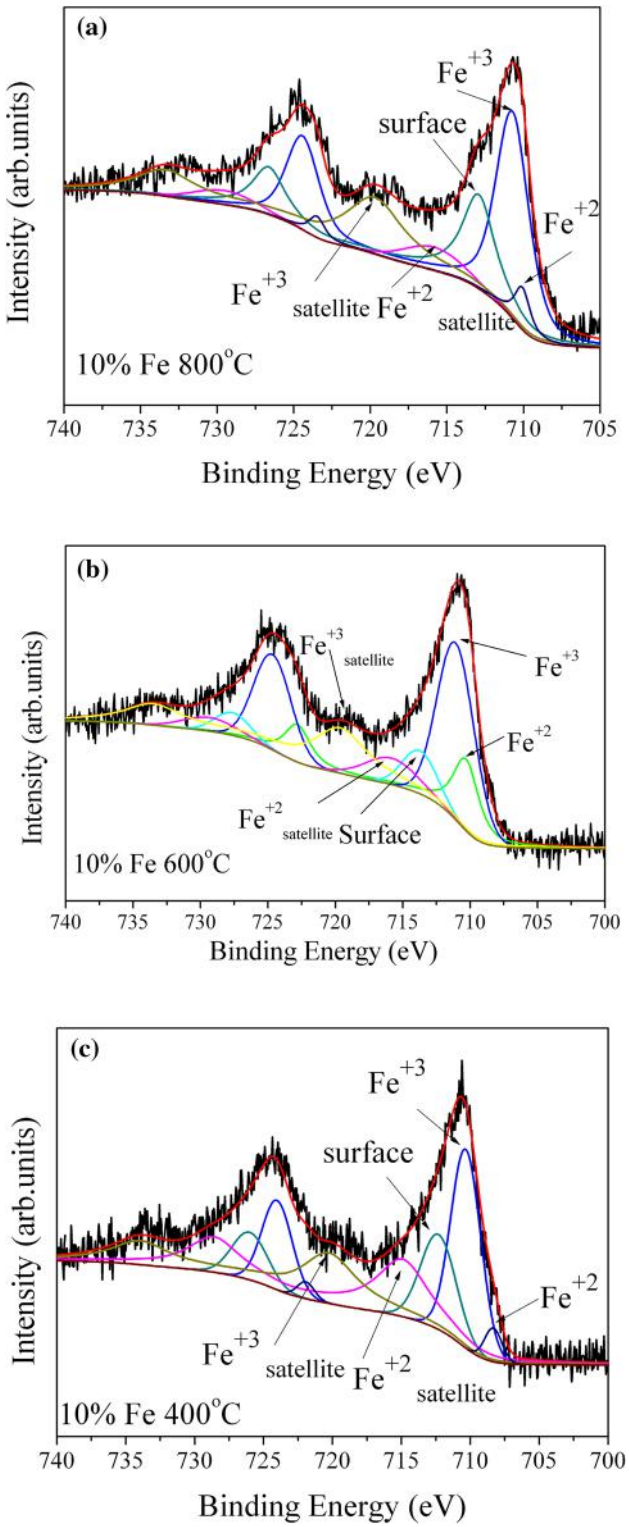

Fig. 9 High resolution XPS core level spectrum of 10% Fe annealed at 800 °C, 600 °C, and 400 °C

ions were found to be dominant in the surface region of nanoaprticles. The shift in binding energies of Fe^{3+} was established upon increasing annealing temperature from 400 to 800 °C. Fe ions in this work were successfully doped into TiO_2 lattice and Fe concentration up to 10% did not exceed the saturation limit.

Table 4 Summary of the Fe 2p peaks position

	$2P_{3/2}$ (FWHM)	Satellite (FWHM)	Oxidation state
1% Fe_400 °C	705.9 (2.40)	–	Fe^0 or defect
	709.0 (1.42)	716.5 (4.9)	Fe^{2+}
	709.7 (1.81)		
	711.4 (4.2)	720.4 (4.9)	Fe^{3+}
	715.2 (3.13)	–	Surface
1% Fe_600 °C	708.5 (1.4)	715.7 (4.5)	Fe^{2+}
	710.3 (3.0)	720.3 (4.0)	Fe^{3+}
	712.8 (3.0)	–	Surface
1% Fe_800 °C	710.4 (2.1)	716.5 (4.5)	Fe^{2+}
	711.8 (4.1)	720.1 (4.5)	Fe^{3+}
	715.5 (4.9)	–	Surface
3% Fe_400 °C	710.43 (0.90)	715.42 (3.47)	Fe^{2+}
	710.78 (3.50)	719.46 (5.50)	Fe^{3+}
	713.55 (2.58)		Surface
3% Fe_600 °C	710.38 (1.9)	716.48 (5.4)	Fe^{2+}
	710.87 (3.56)	720.30 (4.5)	Fe^{3+}
	713.41 (3.00)	–	Surface
3% Fe_800 °C	710.3 (1.20)	716.9 (4.5)	Fe^{2+}
	711.0 (3.30)	720.0 (4.5)	Fe^{3+}
	713.5 (3.00)	–	Surface
5% Fe_400 °C	709.6 (2.50)	716.3 (4.0)	Fe^{2+}
	711.3 (3.62)	720.1 (4.5)	Fe^{3+}
	714.0 (2.57)	–	Surface
5% Fe_600 °C	710.5 (1.74)	716.4 (4.0)	Fe^{2+}
	711.4 (3.37)	720.0 (4.5)	Fe^{3+}
	714.4 (2.57)	–	Surface
5% Fe_800 °C	710.1 (2.08)	717.4 (4.5)	Fe^{2+}
	711.4 (3.94)	720.3 (4.5)	Fe^{3+}
	715.0 (3.35)	–	Surface
8% Fe_400 °C	708.54 (1.35)	715.01 (4.35)	Fe^{2+}
	710.61 (2.76)	719.53 (4.96)	Fe^{3+}
	713.54 (3.15)	–	Surface
8% Fe_600 °C	710.2 (1.70)	715.5 (4.0)	Fe^{2+}
	711.2 (3.14)	719.4 (4.0)	Fe^{3+}
	713.7 (4.00)	–	Surface
8% Fe_800 °C	710.17 (1.64)	716.26 (4.62)	Fe^{2+}
	711.41 (3.63)	719.91 (3.96)	Fe^{3+}
	713.41 (1.36)	–	Surface
10% Fe_400 °C	708.33 (1.4)	714.89 (4.50)	Fe^{2+}
	710.32 (2.53)	720.25 (4.9)	Fe^{3+}
	712.30 (3.00)	–	Surface
10% Fe_600 °C	710.3 (2.20)	716.0 (4.5)	Fe^{2+}
	711.1 (3.20)	719.6 (4.9)	Fe^{3+}
	713.7 (3.00)	–	Surface
10% Fe_800 °C	710.07 (1.08)	715.83 (4.5)	Fe^{2+}
	710.71 (2.5)	719.69 (4.5)	Fe^{3+}
	712.92 (2.5)	–	Surface

References

1. C.E. McCold, Q. Fu, S. Hihath, J.M. Han, Y. Halfon, R. Faller, K. van Benthem, L. Zang, J. Hihath, Ligand exchange based molecular doping in 2D hybrid molecule-nanoparticle arrays: length determines exchange efficiency and conductance change. Mol. Syst. Des. Eng. **2**, 440–448 (2017)
2. B.M. Reddy, I. Ganesh, A. Khan, Stabilization of nanosized titania-anatase for high temperature catalytic applications. J. Mol. Catal. A **223**, 295–304 (2004)
3. W.Y. Choi, A. Termin, M.R. Hoffmann, The role of metal ion dopants in quantum-sized TiO_2: correlation between photoreactivity and charge carrier recombination dynamics. J. Phys. Chem. **84**, 13669–13679 (1994)
4. M. Yeganeh, N. Shahtahmasebi, A. Kompany, M. Karimipour, F. Razavi, N.H.S. Nasralla, L. Šiller, The magnetic characterization of Fe doped TiO_2 semiconducting oxide nanoparticles synthesized by sol-gel method. Phys. B **511**, 89–98 (2017)
5. J.F. Zhu, W. Zheng, B. He, J.L. Zhang, M. Anpo, Characterization of Fe-TiO_2 photocatalysts synthesized by hydrothermal method and their photocatalytic reactivity for photodegradation of XRG dye diluted in water. J. Mol. Catal. A **216**, 35–43 (2004)
6. S. Liu, Y.C.X. Liu, R. Jiang, A novel preparation of highly active iron-doped titania photocatalysts with a p–n junction semiconductor structure. J. Alloys Compd. **506**, 877–882 (2010)
7. J. Zhu, F. Chen, J. Zhang, H. Chen, M. Anpo, Fe^{3+}-TiO_2 photocatalysts prepared by combining sol-gel method with hydrothermal treatment and their characterization. J. Photochem. Photobiol. A **180**, 196–204 (2006)
8. Y. Matsumoto, M. Murakami, T. Shono, T. Hasegawa, T. Fukumura, M. Kawasaki, P. Ahmet, T. Chikyow, S.Y. Koshihara, H. Koinuma, Room-temperature ferromagnetism in transparent transition metal-doped titanium dioxide. Science **291**, 854–856 (2001)
9. M. Crisan, M. Raileanu, N. Dragan, D. Crisan, A. Ianculescu, I. Nitoi, P. Oancea, S. Somacescu, N. Stanica, B. Vasile, C. Stan, Sol-gel iron-doped TiO_2 nanopowders with photocatalytic activity. Appl. Catal. A **504**, 130–142 (2015)
10. J. Yan, G. Wu, N. Guan, L. Li, Z. Li, X. Cao, Understanding the effect of surface/bulk defects on the photocatalytic activity of TiO_2: anatase versus rutile. Phys. Chem. Chem. Phys. **15**, 10978–10988 (2013)
11. B. Santara, P.K. Giri, S. Dhara, K. Imakita, M. Fujii, Oxygen vacancy-mediated enhanced ferromagnetism in undoped and Fe-doped TiO_2 nanoribbons. J. Phys. D **47**, 235304 (2014)
12. I. Ganesh, P.P. Kumar, A.K. Gupta, P.S.C. Sekhar, K. Radha, G. Padmanabham, G. Sundararajan, Preparation and characterization of Fe-doped TiO_2 powders for solar light response and photocatalytic applications. Process. Appl. Ceram. **6**, 21–36 (2012)
13. S. Zhu, W. Liu, C. Fan, Y. Li, Mössbauer study of nano-TiO_2 doped with Fe. Hyperfine Interact. **165**, 273–278 (2005)
14. S.K.S. Patel, S. Kurian, N.S. Gajbhiye, Room-temperature ferromagnetism of Fe-doped TiO_2 nanoparticles driven by oxygen vacancy. Mater. Res. Bull. **48**, 655–660 (2013)
15. Q. Wu, Q. Zheng, R. Krol, Creating oxygen vacancies as a novel strategy to form tetrahedrally coordinated Ti^{4+} in Fe/TiO_2 nanoparticles. J. Phys. Chem. C **116**, 7219–7226 (2012)
16. T. Ali, P. Tripathi, A. Azam, W. Raza, A.S. Ahmed, A. Ahmed, M. Muneer, Photocatalytic performance of Fe-doped TiO_2 nanoparticles under visible-light irradiation. Mater. Res. Express **4**, 015022 (2017)
17. H. Moradi, A. Eshaghi, S.R. Hosseini, K. Ghani, Fabrication of Fe-doped TiO2 nanoparticles and investigation of photocatalytic decolorization of reactive red 198 under visible light irradiation. Ultrason. Sonochem. **32**, 314–319 (2016)

18. A.N. Mangham, N. Govind, M.E. Bowden, V. Shutthanandan, A.G. Joly, M.A. Henderson, S.A. Chambers, Photochemical properties, composition, and structure in molecular beam epitaxy grown Fe "doped" and (Fe,N) codoped rutile TiO_2 (110). J. Phys. Chem. C **115**, 15416–15424 (2011)
19. N.D. Abazovic, L. Mirenghi, I.A. Jankovic, N. Bibic, D.V. Šojic, B.F. Abramovic, M. Comor, Synthesis and characterization of rutile TiO_2 nanopowders doped with iron ions. Nanoscale Res. Lett. **4**, 518–525 (2009)
20. P. Esparza, T. Hernández, M.E. Borges, M.C. Álvarez-Galván, J.C. Ruiz-Morales, J.L.G. Fierro, TiO_2 modifications by hydrothermal treatment and doping to improve its photocatalytic behaviour under visible light. Catal. Today **210**, 135–141 (2013)
21. L.Y. Zhu, X.T. Liu, W.W. Qin, X.S. Liu, N.N. Cai, X.Q. Wang, X.J. Lin, G.H. Zhang, D. Xu, Preparation, characterization and electronic structures of Fe-doped TiO_2 nanostructured fibers. Mater. Res. Bull. **48**, 2737–2745 (2013)
22. A.B. Grosvenor, B.A. Kobe, M.C. Biesinger, N.S. Mclntyre, Investigation of multiplet splitting of Fe 2p XPS spectra and bonding in iron compounds. Surf. Interface Anal. **36**, 1564–1574 (2004)
23. M. Mullet, V. Khare, C. Ruby, XPS study of Fe(II) Fe(III)(oxy) hydroxycarbonate green rust compounds. Surf. Interface Anal. **40**, 323–328 (2008)
24. Y. Wu, J. Zhang, L. Xiao, F. Chen, Properties of carbon and iron modified TiO_2 photocatalyst synthesized at low temperature and photodegradation of acid orange 7 under visible light. Appl. Surf. Sci. **256**, 4260–4268 (2010)
25. J. Yu, Q. Xiang, M. Zhou, Preparation, characterization and visible-light-driven photocatalytic activity of Fe-doped titania nonorods and first-principles study of electronic structures. Appl. Catal. B **90**, 595–602 (2009)
26. J. Zhang, X. Chen, Y. Shen, Y. Li, Z. Hu, J. Chu, Synthesis, surface morphology, and photoluminescence properties of anatase iron-doped titanium dioxide nano-crystalline films. Phys. Chem. Chem. Phys. **13**, 13096–13105 (2011)
27. E. McCafferty, J.P. Wightman, Determination of the concentration of surface hydroxyl groups on metal oxide films by a quantitative XPS method. Surf. Interface Anal. **26**, 549–564 (1998)
28. S. Doniach, M. Šunjic, Many-electron singularity in X-ray photoemission and X-ray line spectra from metals. J. Phys. C **3**, 285 (1970)
29. J. Di'az, G. Paolicelli, S. Ferrer, F. Comin, Separation of the sp^3 and sp^2 components in the C 1s photoemission spectra of amorphous carbon films. Phys. Rev. B **54**, 8064 (1996)
30. D.A. Shirley, High-resolution X-ray photoemission spectrum of the valence bands of gold. Phys. Rev. B **5**, 4709 (1972)
31. Q. Fu, J. Chen, C. Shi, D. Ma, Room-temperature sol–gel derived molybdenum oxide thin films for efficient and stable solution-processed organic light-emitting diodes. ACS Appl. Mater. Interfaces **5**(13), 6024–6029 (2013)
32. J.F. Moudler, W.F. Stickle, P.E. Sobol, K.D. Bomben, *Handbook of X-ray Photoelectron Spectroscopy* (Perkin-Elmer Corp, Eden Prairie, 1992)
33. J.T. Mayer, U. Diebold, T.E. Madey, E. Garfunkel, Titanium and reduced titania overlayers on titanium dioxide (110). J. Electron Spectrosc. Relat. Phenom. **73**, 1–11 (1995)
34. U. Diebold, The surface science of titanium dioxide. Surf. Sci. Rep. **48**, 53–229 (2003)
35. D.A.H. Hanaor, I. Chironi, I. Karatchevtseva, G. Traini, C.C. Sorrell, Single and mixed phase TiO_2 powders prepared by excess hydrolysis of titanium alkoxide. Adv. Appl. Ceram. **111**, 149–158 (2012)
36. E.A. Kozlova, T.P. Korobkina, A.V. Vorontsov, V.N. Parmon, Enhancement of the O_2 or H_2 photoproduction rate in a Ce^{3+}/Ce^{4+}-TiO_2 system by the TiO_2 surface and structure modification. Appl. Catal. A **367**, 130–137 (2009)
37. J.F. Porter, Y.G. Li, C.K. Chan, The effect of calcination on the microstructural characteristics and photoreactivity of Degussa P-25 TiO_2. J. Mater. Sci. **34**, 1535–1545 (1999)
38. N.L. Wu, M.S. Lee, Z.J. Pon, J.Z. Hsu, Effect of calcination atmosphere on TiO_2 photocatalysis in hydrogen production from methanol/water solution. J. Photochem. Photobiol. A **163**, 277–280 (2004)
39. P.R. Ettireddy, N. Ettireddy, S. Mamedov, P. Boolchand, P.G. Smirniotis, Surface characterization studies of TiO_2 supported manganese oxide catalysts for low temperature SCR of NO with NH_3. Appl. Catal. B **76**, 123–134 (2007)
40. X. Weimiao, C. Hui, Z. Xuanhui, H. Xianchao, L. Guohua, Preparation and photocatalytic activity of rutile TiO_2 and goethite composite photocatalysts. Chin. J. Catal. **34**, 1076–1086 (2013)
41. J.T. Kloprogge, L.V. Duong, B.J. Wood, R.L. Frost, J. Colloid Interface Sci. **296**, 572–576 (2006)
42. F.F.H. Aragon, J.D. Ardisson, J.C.R. Aquino, I. Gonzalez, W.A.A. Macedo, J.A.H. Coaquira, J. Mantilla, S.W.D. Silva, P.C. Morais, Effect of the thickness reduction on the structural, surface and magnetic properties of α-Fe_2O_3 thin films. Thin Solid Films **607**, 50–54 (2016)
43. J.T. Carneiro, T.J. Savenije, J.A. Moulijn, G. Mul, Toward a physically sound structure—activity relationship of TiO_2-based photocatalysts. J. Phys. Chem. C **114**, 327–332 (2010)
44. M. Hirano, T. Joji, M. Inagaki, H. Iwata, Direct formation of iron(III)-doped titanium oxide (anatase) by thermal hydrolysis and its structure property. J. Am. Ceram. Soc. **87**, 35–41 (2004)
45. J. Yu, M. Zhou, H. Yu, Q. Zhang, Y. Yu, Enhanced photoinduced super-hydrophilicity of the sol–gel-derived TiO_2 thin films by Fe-doping. Mater. Chem. Phys. **95**, 193–196 (2006)
46. C.C. Yen, D.Y. Wang, L.S. Chang, H.C. Shih, Characterization and photocatalytic activity of Fe- and N-co-deposited TiO_2 and first-principles study for electronic structure. J. Solid State Chem. **184**, 2053–2060 (2011)
47. M. Muhler, R. Schlogl, G. Ertl, The nature of the iron oxide-based catalyst for dehydrogenation of ethylbenzene to styrene 2. Surface chemistry of the active phase. J. Catal. **138**, 413–444 (1992)
48. N.N. Greenwood, A. Earnshaw, *Chemistry of the Elements*, 2nd edn. (Butterworth-Heinemann, Amsterdam, 1997)
49. V.E. Heinrich, P.A. Cox, *The Surface Science of Metal Oxides* (Cambridge University Press, Cambridge, 1994)
50. T. Tong, J. Zhang, B. Tian, F. Chen, D. He, Preparation of Fe^{3+}-doped TiO_2 catalysts by controlled hydrolysis of titanium alkoxide and study on their photocatalytic activity for methyl orange degradation. J. Hazard. Mater. **155**, 572–579 (2008)
51. H.W. Nesbitt, I.J. Muir, X-ray photoelectron spectroscopic study of a pristine pyrite surface reacted with water vapour and air. Geochim. Cosmochim. Acta **58**, 4667–4679 (1994)
52. T. Droubay, S.A. Chambers, Surface-sensitive Fe 2p photoemission spectra for α-Fe_2O_3(0001): the influence of symmetry and crystal-field strength. Phys. Rev. B **64**, 205414 (2001)
53. S. Hüfner, *Photoelectron Spectroscopy: Principles and Applications* (Springer, Berlin, 2003)
54. J.M.D. Coey, M. Venkatesan, C.B. Fitzgerald, Donor impurity band exchange in dilute ferromagnetic oxides. Nat. Mater. **4**, 173–179 (2005)